How to build a fast and accurate Code-Modulated Brain-Computer Interface

Authors[1].

[1] Institution

E-mail: xxx@xxx.xx

Received xxxxxx
Accepted for publication xxxxxx
Published xxxxxx

Abstract

Objective. In the last decade, the advent of code-modulated brain-computer interfaces (BCIs) has allowed the implementation of systems with high information transfer rates (ITRs) and increased the possible practicality of such interfaces. In this paper, we evaluate the effect of different numbers of targets in the stimulus display, modulation sequences generators, and signal processing algorithms on the accuracy and ITR of code-modulated BCIs. *Approach*. We use both real and simulated EEG data, to evaluate these parameters and methods. Then, we compared numerous different setups to assess their performance and identify the best configurations. We also evaluated the dependability of our simulated evaluation approach. *Main results*. Our results show that Golay, Almost Perfect, and deBruijn sequence-based visual stimulus modulations provide the best results, significantly outperforming the commonly used m-Sequences in all cases. We conclude that artificial neural network processing algorithms offer the best processing pipeline for this type of BCI, achieving a maximum classification accuracy of 94.7% on real EEG data while obtaining a maximum ITR of 127.2 bits/min in a simulated 64-target system. *Significance.* We used a simulated framework that demonstrated previously unattainable flexibility and convenience while staying reasonably realistic. Furthermore, our findings suggest several new considerations which can be used to guide further code-based BCI development.

Keywords: Brain-Computer Interface, Code Modulated Visual-Evoked Potentials, Canonical Correlation, Artificial Neural Networks, m-Sequence, Almost Perfect Autocorrelation, DeBruijn, Golay Sequence.

1. Introduction

Electroencephalographic (EEG) data is acquired by measuring the net synaptic excitations from the surface of the scalp [1]. Components of the EEG elicited by exogenous stimuli, known as event-related potentials (ERPs), are commonly used in brain-computer interfaces (BCI) to identify control commands, allowing BCI users to communicate without motor or peripheral interaction [2]. These benefits have led to the accelerated pursuit of high-performance BCI systems in the last two decades [3][4][5][6].

Modern BCIs are frequently based on the neural potentials evoked by out-of-sequence or unexpected time-dependent external events, such as P300 event-related potential-based systems, or by the response to frequency-dependent visual or auditory stimuli, like steady-state visual-evoked potentials (SSVEPs) [7]. Both types of BCI operate by presenting stimuli to the user which alternates in appearance at regular intervals. ERP-based BCIs are more comfortable to use, while SSVEP BCIs offer better performance in terms of accuracy and speed of the BCI [8][9].

In addition to the ERP and SSVEP types of BCI, systems based on code-modulated visual evoked potentials (c-VEPs) have gained relevance more recently as a proposed solution to the issues of visual fatigue and sub-optimal information transfer rates in users of several ERP and SSVEP-based BCIs [3][8][10][11].

By modulating the display of an array of visual stimuli with a predetermined pseudorandom binary sequence (PRBS) at relatively high and uniform frequencies such as 60 and 120 Hz [3][12], BCIs based on c-VEP offer the potential for much more pleasant operation [10]. Although there are several methods for generating a PRBS, there is no definite optimal choice for BCI applications. Numerous types of PRBS have been implemented in this context, for example, m-Sequences [3] [8] [12] [13], Almost Perfect Autocorrelation [14] sequences, and Gold sequences have all been attempted [15].

The structure of the interface display used with c-VEP BCIs is similar to the interface typically used with other VEP-based BCIs and commonly consists of a rectangular arrangement of multiple square target cells surrounded by complementary non-target cells. By adopting the principle of equivalent neighbors [16] and the comments by Bin *et al.* [17] regarding the VEP field of view, it is reasonable to display all these stimulus sources in a compactly arranged grid on a display screen.

Besides reducing visual fatigue, several different c-VEP BCIs have been proposed which typically outperform the information transfer rates (ITRs) obtained with SSVEP-based systems. For example, in 2009 Bin *et al.* [17] obtained an information transfer rate of 58±9.6 bit/min with an SSVEP-based BCI, but later in 2010 proposed a c-VEP system that achieved a much higher average ITR of 108±12 bits/min [3]. Two years later, this high ITR score was further improved by Spüler *et al.* [7], reaching 144 bit/min with a BCI that also incorporated error-related potentials, allowing online adaptation. In 2018, Wei *et al.* [14] proposed a novel c-VEP BCI structure based on grouped stimulus targets, yielding an even higher ITR of 181.05 bits/min.

Several parameters influence the efficacy of a c-VEP BCI. They include but are not limited to, the type of PRBS used to present the stimuli, the feature extraction process used within the signal processing pipeline, and the number of targets presented to the user. Many different variants of these parameters have been investigated by c-VEP BCI researchers. However, to date, there is no clear consensus on which parameters are most effective in allowing the construction of a fast and accurate c-VEP BCI.

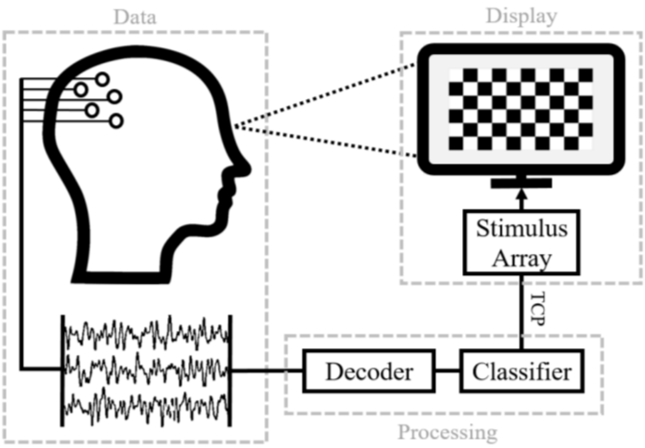

Figure 1. The workflow overview diagram of the c-VEP BCI system, composed of three stages executed cyclically: data acquisition, signal processing, and visual stimulation.

In this paper, we work with a high-speed c-VEP BCI framework using both a real EEG dataset and a simulated EEG dataset. We evaluate the effect of multiple PRBS types, signal processing algorithms, and numbers of stimuli in the presentation setup on the overall performance of the c-VEP BCI system, measured through accuracy and ITR. We also compare various attributes between the experimental and the simulated EEG datasets to assess the dependability of the simulation approach.

2. Methods

2.1 Theory of Operation

Figure 1 shows the workflow overview diagram of a typical c-VEP BCI system. It is composed of three stages executed cyclically: data acquisition, signal processing, and visual stimulation. The interface first presents multiple command options to the user. Each of these commands displayed is modulated, over time, by the PRBS. For example, commands may be toggled between two different states (e.g. visible vs. hidden, or greyed out vs. highlighted) according to the digit of each bit in the PRBS. For the signal processing stage, as is generally the case [5], the system acquires the c-VEP data from the user, processes the multi-channel signals in the time and spatial domains, extracting the relevant features, to finally perform the identification as to which stimulus source the user is fixating on, and ultimately execute the command of the user's interest without physical interaction with the machine.

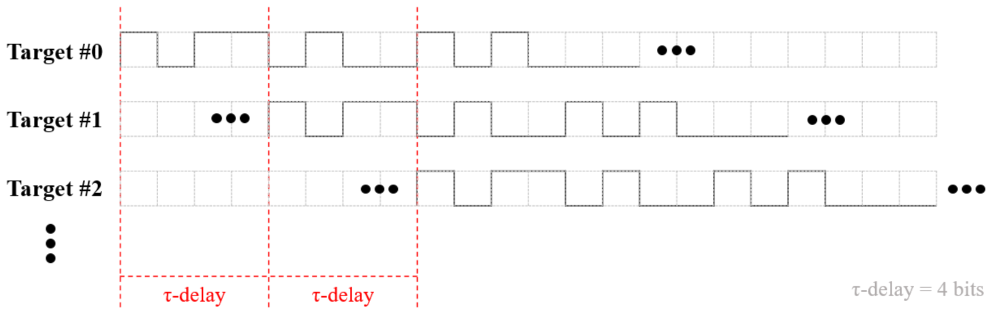

Figure 2. Visualization of an example of the modulation behavior of the first three stimulus targets, showing a consecutive circular shift of 4 bits of the same pseudorandom binary sequence

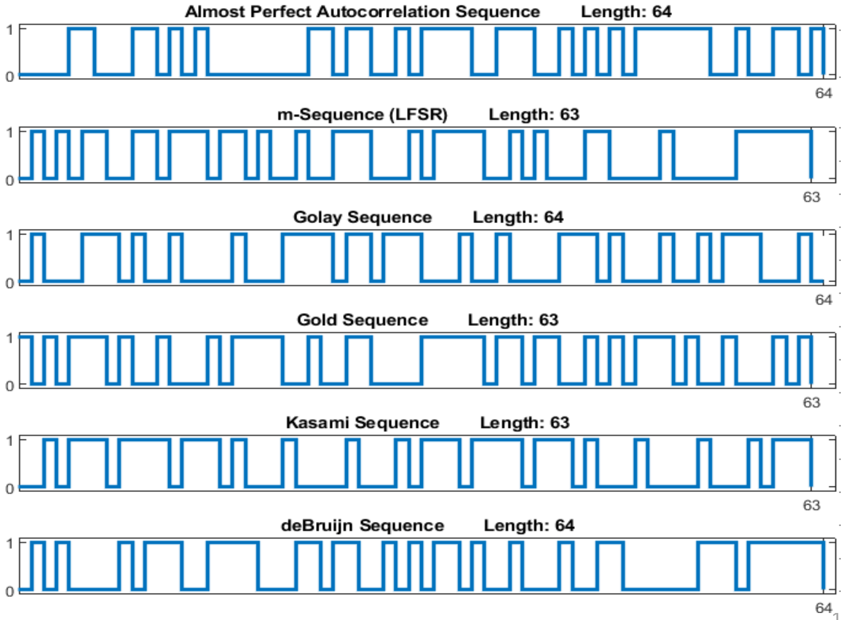

Figure 3. Instances of modulation sequences visualized. Examples of the six distinct PRBS evaluated in a 64-bit setup, from top to bottom: APA, m-Sequence, Golay, Gold, Kasami, and DeBruijn sequences.

In this study we supersede the data acquisition and display stages by employing an offline BCI, that is, by using pre-recorded real and pre-generated synthetic EEG, allowing us to focus on the processing pipeline. Specifically, we utilized a signal simulation program (developed in MATLAB R2019b) for EEG signal simulation, inspired by the open-source framework developed by Lindgren *et al.* in 2018 [18]. While for the real EEG, we used a dataset provided by Wei *et al.* [14].

As shown in *Figure 2*, the behavior of each target stimuli presented to the user is modulated frame by frame with a consecutively shifted PRBS, in which the 0/1 value of the momentary bit toggles a particular stimulus on and off, as suggested by Wei *et al.* [19]:

$$M(t)_{Tar_i} = PRBS\left(t + \left(i * \tau_{delay}\right)\right) \qquad (eq.1)$$

where M is the binary value of target i (Tar_i) at time t, considering a τ lag of 4 bits between consecutive targets, and $PRBS(x)$ defines digit x of the stimuli modulation sequence in the BCI setup.

To evaluate the effect of different configurations on the system performance we explored multiple options for three key parameters from the typical c-VEP BCI setup and processing pipeline. First, we used three distinct numbers of targets (16, 32, and 64 targets). This choice of numbers of available targets was based on the comments made by Baseler *et al.* [20] describing the negative impact on performance from an increase of targets presented to users in a BCI. Second, we evaluated 6 of the most widely used types of PRBS for modulation of the stimuli (detailed in *section 2.3*). Finally, we implemented 6 decoding algorithms that are commonly used in the context of BCI feature extraction (*section 2.4*).

2.2 Data Acquisition

2.2.1 Experimental Approach

The experimental dataset, provided by Wei et al [14], consisted of two independent c-VEP data subsets recorded from 12 different c-VEP BCI users (8 females) with normal or corrected to normal vision, between the ages of 21 and 26 years old. In the training subset, users fixated on one particular target from the array, defined as the reference target, for 20 trials, effectively providing 240 training trials in total. In the testing subset, each of the 12 participants fixated on each target from an array of 16 square targets, for 5 useful cycles of the stimuli modulation sequence each, totaling at 960 distinct trials.

The setup for the acquisition of the real experimental EEG data utilized an almost perfect autocorrelation (APA) sequence of length 64 bits with frequency modulation of 60Hz and a sampling rate of 1000Hz. The electrode impedances were <10kΩ and EEG electrodes were placed at positions P3, Pz, P4, PO7, POz, PO8, O1, Oz, and O2 in the international 10/20 system for EEG electrode placement.

2.2.2 Simulated Approach

Using the EEG simulator program, we generated an extensive synthetic EEG dataset for use in our analysis, consisting of two independent subsets for training and testing data, with a total of 240 and 1920 trials respectively, mirroring the structure from the experimental EEG dataset, while doubling the extent of the testing data.

The generation of the artificial EEG signals consisted of a composite of three elements: the purely code-modulated responses to the PRBS stimulation, white and pink noise originating uniformly from the scalp surface and the head volume, respectively, with internal signal-to-noise-ratios of 1 and 0.8, as suggested in [18]. We also added heuristically-sourced eye movement and eye blink noise artifacts, which in the simulation were set to occur at random times within the trial with probabilities of 30% and 10% respectively, and have random lengths of between 0 (i.e. non-existent) and 2 seconds, as proposed by Tangermann *et al.* [21]. This signal was passed through a 2-45Hz bandpass filter to limit the data to the frequency bands of interest, resulting in the final simulated EEG.

To calibrate the proportions between the noise components and the purely evoked responses, we incorporated a global signal-to-noise ratio (SNR) coefficient into the simulator. We tuned the SNR to maximize the resemblance of the performance results between both approaches and those

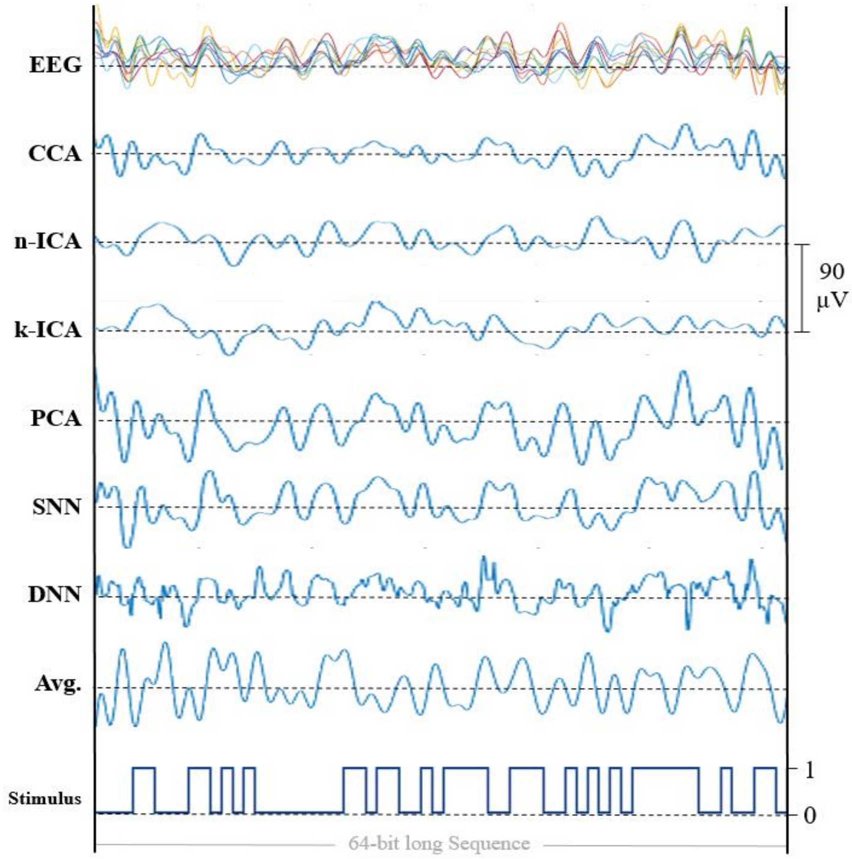

Figure 4. Comparison of single-cycle signals. From top to bottom: Raw EEG signal, pre-processed signal outputs of the six decoding algorithms, the signal average from 20 cycles, and an APA modulation sequence with a length of 64 bits.

obtained by Wei *et al* [14] using an identical setup in simulation. Once tuned, the global SNR coefficient was set to a unitary value to later analyze the performance of our BCI with a range of SNR values (from 0.2 to 2 dB) and observe how influential this simulation parameter is. These results are shown in *Figure 9* and detailed in *section 3*.

Finally, the modulation frequency and the sampling rate were set to 60Hz and 1000Hz, respectively, and the simulated EEG electrodes were placed in the same positions as those from the experiments, following the international 10/20 system for EEG electrode placement: P3, Pz, P4, PO7, POz, PO8, O1, Oz, and O2. To achieve this in simulation, the signal generation is based on a linear superposition model that uses a leadfield matrix encoding the electrical propagation of the head model [18]. We work with a physiologically realistic non-specific brain model, which projects uniform brain volume data to the surface electrodes, constrained by the cortical surface normal. The conductivity parameters of the model consist of scalp, skull, and brain mesh layers, with normalized conductivities of 1, 1/15, and 1, respectively, per Oostendorp *et al.* [22]. Finally, this head model also contains the dipole sources located at the front of the head representing the users' eyes, from which the previously mentioned eye noise artifacts are set to originate.

2.3 Modulation Sequences

Six different PRBS were selected. These modulation sequences (MS) were chosen because they all are deterministically generated and have desirable statistical properties, such as low autocorrelation, despite the non-linear influence that these characteristics have on VEPs [3]. The sequences used in this study were: Linear-feedback shift register (LFSR, also known as m-Sequences), deBruijn, Almost Perfect Autocorrelation, Golay, Gold, and Kasami sequences. Examples of each of these MS are shown in *Figure 3*. The sequences are generated through brute computational methods and/or distinct recursive algorithms. This is the case for LFSR and DeBruijn sequences where, for instance, the following primitive polynomials (mod 2 and 3 respectively) can be used recursively to generate both of these PRBS:

$$f(x)_{LFSR} = x^4 + x^3 + x^2 + 1 \qquad (eq.2)$$

$$f(x)_{deBruijn} = x^4 + 2x + 2 \qquad (eq.3)$$

where the exponents of each *x* term (also referred to as *taps*), represent the non-zero bit positions influencing the feedback for the next state in the recursive arrangement. In this case, the polynomial degree of n=4 results in a PRBS of 15 (2^n-1) and 16 (2^n) bits in length, respectively.

Each of these MS is commonly used in cryptography and spectrometry [23], neurological research [8] [24], and communication systems [25] due to their semi-random statistical properties [26] [27]. Furthermore, DeBruijn sequences have been beneficial for neural decoding processes in the wider neuroscientific context ([4]). While m-Sequences are perhaps the most frequently implemented type of MS in the context of c-VEP BCI research ([3] [8] [12] [13]), Golay and APA sequences have also been successfully implemented in novel c-VEP paradigms ([14]). Although to a lesser extent, Gold sequences have also previously been explored by Thielen *et. al.* [15] in another VEP-based paradigm consisting of asynchronously evoked Broad-band VEPs, due to the optimal cross-correlation properties of such sequences. Similarly, while Kasami sequences have had a highly limited presence in BCI research, these demonstrated inconclusive results in the context of c-VEP modulation when studied in 2017 by Isaksen *et al.* [28].

2.4 Decoding Algorithms

Multiple decoding algorithms were implemented to assess their effectiveness at decluttering an EEG signal through feature extraction.

In our evaluation of the c-VEP processing pipeline, we use six of the most commonly used decoders for EEG feature extraction [8] [13] [29] [30]. The feature algorithms implemented are Canonical correlation analysis (CCA), principal component analysis (PCA), independent component analysis with maximum kurtosis (k-ICA) and maximum negative entropy criterion (n-ICA), shallow (SNN), and deep neural networks (DNN).

We used these algorithms to perform a translation from the multidimensional raw EEG signal to a one-dimensional processed feature signal. Each of the algorithms is described in the following sections. The resulting processed one-dimensional feature set was then passed to the classification phase, thus identifying which c-VEP target stimuli the user was attending to in a given trial (described in *section 2.5*).

2.4.1 Canonical Correlation Analysis

The CCA algorithm was utilized to create the spatial filter:

$$y[n] = \sum_{i=1}^{C} x_i[n]\, w_{xi} \qquad (eq.4)$$

where $x_i[n]$ represents the n-th element of the i-th channel (i= 1, 2,…, C) from the multichannel input signal, which, once multiplied by the i-th weight from the set of weights Wx, results in the one-dimensional spatially-filtered signal y. And the set of weights Wx is calculated from the CCA:

$$\max_{W_x, W_y} \frac{W_x^T\, X\, \hat{X}^T\, W_y}{\sqrt{W_x^T X X^T W_x \cdot W_y^T \hat{X} \hat{X}^T W_y}} \qquad (eq.5)$$

where the terms Wx and Wy denote the linear canonical coefficients that maximize the correlation between the unprocessed EEG input X and an averaged multichannel signal replicated for congruency, denoted here as $\hat{X}$, and computed as follows:

$$X = [X_1\ X_2\ X_3\ \cdots\ X_N] \qquad (eq.6)$$

$$\bar{X} = \frac{1}{N} \sum_{i=1}^{N} X_i \qquad (eq.7)$$

$$\hat{X} = [\bar{X}\ \bar{X}\ \bar{X}\ \cdots\ \bar{X}] \qquad (eq.8)$$

where the X input signal is collected from N stimulus cycles and $\bar{X}$ represents the averaged signal before being replicated lengthwise N number of times.

2.4.2 Principal component analysis

Principal component analysis increases the interpretability of the signal X, by identifying a projection of the data such that the new dimensions of the data projected are organized by decreasing variance. The dimensionality of the signal can then be reduced by sub-selecting components from the new projected dimensions [31]. We select and further process only the one principal component with the largest corresponding Eigenvalue, here denoted as W_1:

$$\max_{W_1} \frac{W_1^T X^T X\, W_1}{W_1^T W_1} \qquad (eq.9)$$

which in our testing corresponds to the single projected component of the data that represented 75-90% of the total variance in the case of simulation, and 35-50% for experimental data, indiscriminate of the particular stimulus source or modulation sequence.

2.4.3 Independent component analysis

By assuming that the input X is an initial linear combination of real independent sources, denoted as S, we can use Independent Component Analysis (ICA) to extract a single feature set. These algorithms seek the linear transformation matrix A that transforms the EEG signals X into a new component space Y that approximates S. This is achieved by maximizing the statistical independence between each of the output components. Specifically, each recorded signal trial X is assumed to be a linear mixture of sources:

$$\boldsymbol{X} = \boldsymbol{A} \times \boldsymbol{S} \qquad (eq.10)$$

Where S denotes the original sources and A denotes the linear mixing matrix. An estimate of the sources Y can then be found by inverting the mixing matrix:

$$\boldsymbol{Y} = \boldsymbol{A}^{-1} \times \boldsymbol{X} \qquad (eq.11)$$

ICA has been demonstrated to produce a useful decomposition of EEG signals in numerous BCI applications [29] [32].

However, when using an ICA method the dimensionality of the EEG signal set is not reduced, but maintained. Therefore, it is necessary to define some method to select one of the C independent components of a test trial available for eventual use in classifying the c-VEPs. To accomplish this, we measure the Pearson correlation coefficient between all independent components and all T reference templates produced for the current BCI setup, hence performing T×C computations. Whichever component maximizes the Pearson correlation coefficient with any of the reference templates is selected as the feature of interest for the subsequent classification stage. The generation of said templates is elaborated upon in *section 2.5*, while a discussion on the benefits and caveats of this procedure is included in *section 4.2*.

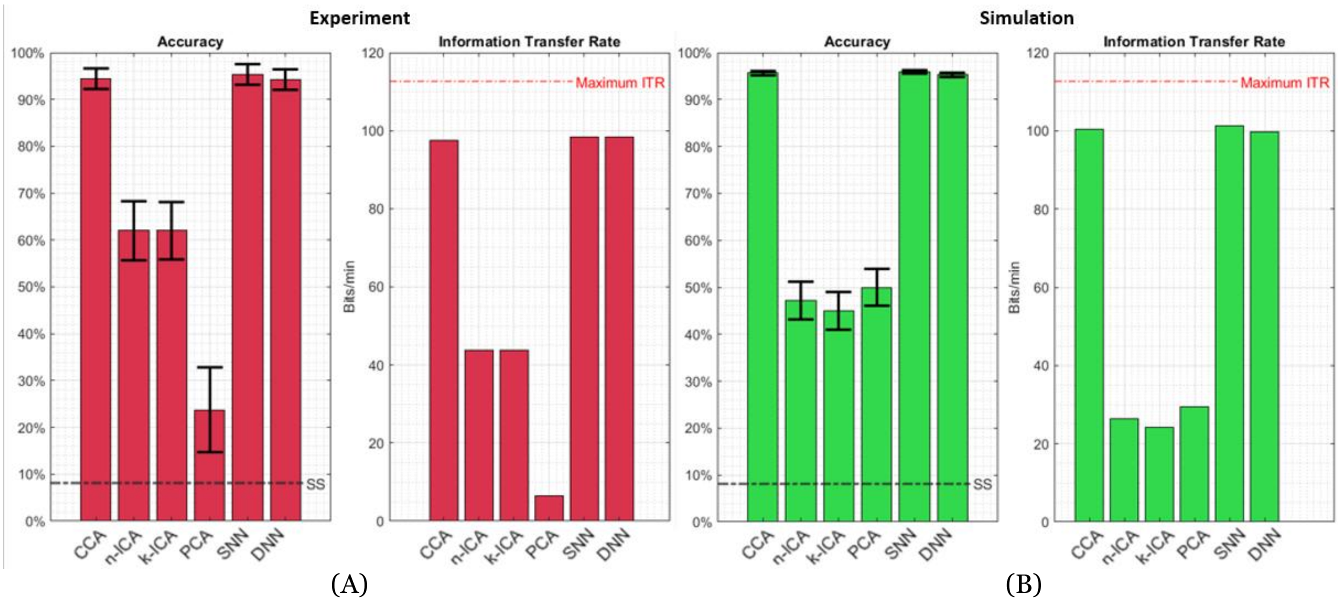

Figure 5. Comparison of experimental and simulated analysis. Results obtained from both experimental *(A)* and simulated *(B)* approaches with the same configuration: APA sequence modulation with a 16-target BCI. The left plots of *(A)* and *(B)* show the accuracies [%] with error bars and statistical significance line with a p-value < 0.01 of a random 16-target classifier. The right plots of *(A)* and *(B)* show the ITR for each decoder [bits/min]. The maximum ITR (red horizontal line) is achieved when the accuracy reaches 100%, resulting in an ITR of 112.5 bits/min.

2.4.4 Artificial neural networks

Although the incorporation of artificial neural networks (ANNs) into c-VEP BCIs is not the most common practice, these methods have previously achieved highly accurate results in a few BCI systems [30] [33] [34]. We evaluated two different multi-layer perceptrons for their computationally light signal processing capacity and their high accuracies [35]. While one consists of 4 hidden layers, with 9, 18, 18, and 9 hidden neurons in each layer respectively; the other network is shallow, consisting of a single 10-neuron hidden layer.

We trained both ANN structures using sigmoid activation and with the same inputs and the summed channels of the outputs with which the CCA-based filter was also generated, but staying independent from the CCA method. That is to say, the training inputs consist of the unprocessed EEG signal X of C-channels (from eq. 6), while the training outputs consisted of the signal $\hat{X}$ (see eq. 8), averaged along the C channels, resulting in a one-dimensional signal, here denoted as H:

$$H = \frac{1}{C}\sum_{i=1}^{C} \hat{x}_i \qquad (eq.12)$$

2.5 Classification and Evaluation

The classification procedure consisted of matching the processed one-dimensional feature set extracted from the EEG signals using each of the previously described decoding algorithms to one template from a set of T reference templates, where T is the number of classes (or targets) in the particular setup. All the necessary templates are obtained from the consecutive circular shift of one reference template, T number of times. This initial reference template is obtained by averaging the EEG data from all the trials collected for the training subset, in the case of the experimental approach; and from the average of all signals generated as the training subset using the simulator, for the simulated approach. Since all stimulus targets are modulated by the same circularly-shifted PRBS, each resulting reference template can be associated with each individual target.

Once all templates are available after the training, the testing phase can be performed. In this phase, whichever reference template has the highest correlation coefficient with the feature set indicates which of the T target positions the BCI user is attempting to select, classifying it as such. Lastly, each of the 18 simulated configurations possible, as well as the decoding algorithms on the real data, were assessed by calculating the accuracy [%], with its variance, and the information transfer rate (ITR) expressed in bits/min.

Beyond evaluating all configuration parameters in the simulated framework, we are interested in assessing the reliability of the framework itself. To carry out this evaluation, we statistically compare the power spectra and the grand average ERPs obtained from both approaches, as well as the SNR-accuracy relationship in simulation. The following section describes the results of all analyses, while a discussion on their significance is contained in *Section 4*.

3. Results

The accuracy and ITR of the offline classification tests carried out on the experimental set are presented in *Figure 5(A)*, while those results achieved by the simulator in an identical setup (16 targets with APA modulation) are contained in *Figure 5(B)*. Also included in both accuracy graphs within *Figure 5* is the variance and statistical significance level ($p < 0.01$), the latter of which is indicated by a dashed horizontal line at 8.13% and represents the accuracy level that we expect less than 1% of a set of random 16-target classifiers to obtain, as assessed against a binomial distribution (see [36]). This figure shows nearly equal scores obtained through both approaches using CCA, SNN, and DNN, reaching accuracies of 94.38%, 95.34%, and 94.22%, in the respective experiments; and 95.63%, 95.94%, and 95.31%, in the respective simulations. Note, while both ICA and the PCA algorithm return much lower scores relative to the rest of the decoders in experiments and simulation, it must be noted that both approaches achieve significantly different scores, which is discussed in *Section 4.2*.

Proceeding with the evaluation through purely simulated means, *Figure 6* condenses the scores obtained by each of the possible BCI setups. From the upper portion of this figure, which contains the accuracies, variance, and significance level of each instance, there is a noticeable decline in the scores as the number of targets is increased. On the other hand, as can be observed from the information transfer rates shown in the lower section of *Figure 6*, this negative tendency is partially counteracted by this same increase in targets, resulting in the net relative increase of ITR with a higher target number.

Concerning the modulation sequence used, Golay sequences produced all of the highest accuracies in the 16-target setups, while Almost Perfect sequences provide the best results of 32 and 64-target configurations above 80%. However, it is worth pointing out that all three Golay, APA, and DeBruijn modulation sequences achieve the most promising results in all cases, frequently without being significantly distant from each other.

Additionally, Linear-feedback shift register (m-Sequences), Gold, and Kasami sequences demonstrated substantially poorer performances in almost all scenarios. In particular, Kasami sequences resulted in an average decrement from the highest accuracy of -50.9%, -44.3%, and -48.5% throughout each of the 64, 32, and 16-target simulated configurations, respectively.

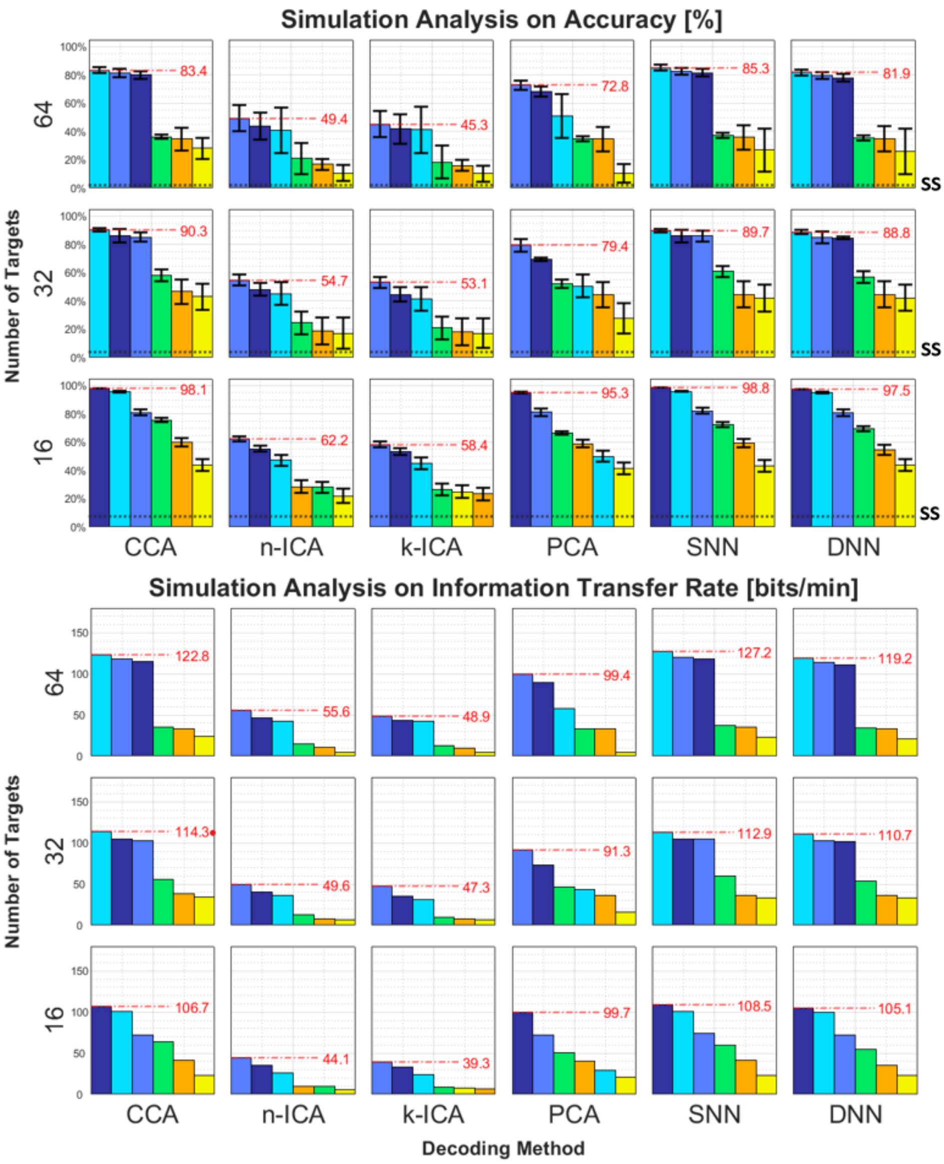

Figure 6. Simulated analysis results summary. (Upper) The accuracies obtained from all possible combinations of decoder, target number, and sequence type, with corresponding variances, and statistical significance levels (with p-value < 0.01) marked with a black dotted lines and the subscript "SS". (Lower) The corresponding ITRs calculated as a function of the number of targets and the accuracy of each setup. Additionally, the red dashed lines mark the maximum scores achieved within each one of the setups.

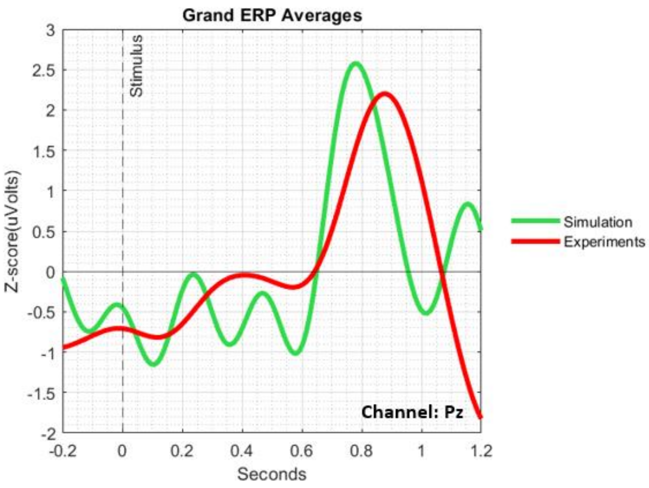

Figure 7. Grand ERP averages, z-scored. Grand ERP average of channel Pz from simulated data (green) and experimental data (red). Both are obtained by averaging over 20 cycles. The visual stimulus is presented at time zero.

Finally, concerning the impact of each feature extraction algorithm, the results demonstrate that both ICA algorithms get remarkably lower scores, while CCA and both NNs represent the most efficient decoding methods. Even though *Figure 6* suggests these three decoders are similarly competent, the SNN notably achieves the highest accuracy of 98.8% with a 16-target Golay setup and the maximum ITR of 127.2 bits/min with an APA 64-target system.

Proceeding with the evaluation of the simulator properties, a comparison of the normalized grand ERP averages and power spectra of both data acquisition approaches is shown in *Figure 7* and *Figure 8*, respectively. We can observe that the morphologies of the positive peaks from the simulated and experimental responses in *Figure 7* are noticeably similar, with no statistically significant difference based on a two-sample t-test with a significance of α=0.05. Still, there is an approximate deviation of 11.9% between both response latencies, and approximately a 14.6% increase in the amplitude of the simulator's ERP relative to the one generated with real EEG data.

Further analysis between signals obtained through both approaches can be done with the power spectra from all 9 electrodes, shown in *Figure 8*. From this figure we can draw two conclusions: the frequency bands are greatly comparable since the relevant portions of both (the 0-50 Hz range approximately) are not statistically different based on a two-sample t-test with a significance level of α=0.05; and that the simulation provides more orderly activation among the electrodes than the real EEG data provides, suggesting unrealistic response distribution among the electrodes, as well as slightly larger amplitudes in the higher frequencies before the cutoff at ~50Hz (i.e. 30-40Hz).

Finally, *Figure 9* is intended to show the influence of the signal-to-noise ratio (SNR) coefficient of the simulator on the accuracy of each feature extractor. As detailed in *section 2.2.2*, a coefficient of 1 was set as a baseline for the SNR that provides the most realistic results, using the experimental data as a reference. The outcomes depicted were obtained by averaging the accuracies scored by the three setups using APA modulation (16, 32, and 64 targets), resulting in an inverted exponential relationship between SNR and the accuracy.

4. Discussion

4.1 On the BCI System

As previously stated, our results show that the SNN and CCA algorithms represent the most promising feature extractors for building c-VEP-based BCIs at a somewhat equal degree, since these achieve the highest scores throughout all numbers of targets without diverging significantly. However, by taking into account the considerably higher computational load and training time required to set up neural networks, we consider CCA a more favorable choice for an online system, especially if computing capacity is of the essence. The consistently inferior performances from the ICA and PCA algorithms suggest that these are not suitable for this type of BCI. Additionally, the correlation-based component selection procedure of ICA feature extraction (described in *Section*

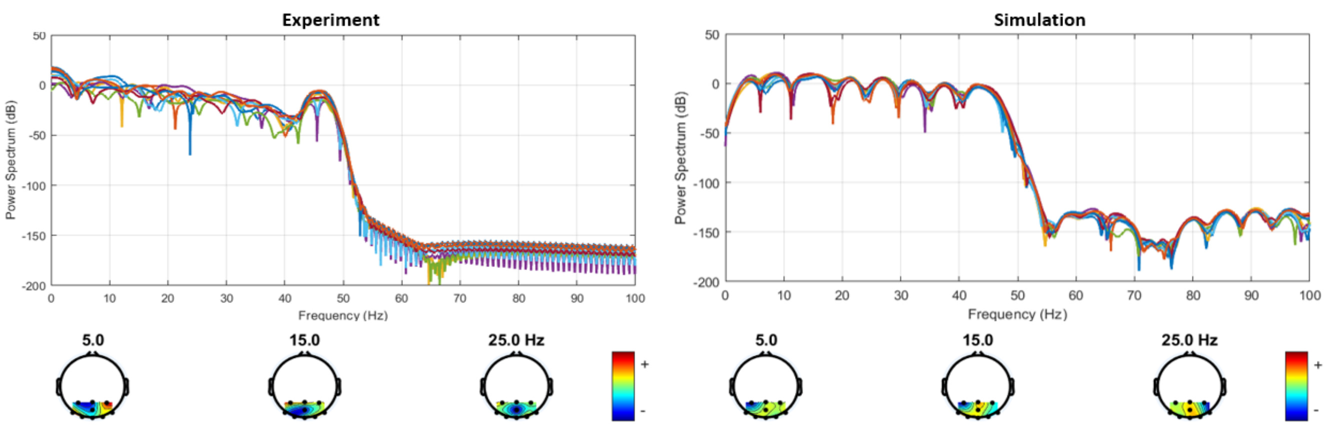

Figure 8. The frequency power spectrum was obtained from experimental (left) and simulated (right) c-VEP datasets. With a topological activation map of the regions with electrodes at 5, 15, and 25 Hz for each approach.

2.4.3) is a non-ideal process in terms of computation, since the number of calculations greatly increases along with an increase in the number of targets, which in an online system represents a reduction of processing speed.

We also conclude that among the PRBS investigated with simulation, Golay, DeBruijn, and Almost Perfect sequences are the most effective for stimuli modulation. While APA sequences are fairly common in c-VEP studies, Golay and DeBruijn sequences have only been implemented to a very limited extent, which prompts a highly interesting hypothesis for further testing through non-simulated means. Furthermore, the consistently suboptimal results obtained with the Kasami, Gold, and m-Sequence PRBS suggest that these have unfavorable characteristics for code-modulated BCIs.

Finally, as indicated earlier, the increase in the number of targets in the BCI results in a noticeable decline in the accuracy of all of the configurations. This highlights the limited scalability of numbers of targets in c-VEP BCI systems, as noted by [14] and [20]. This tendency is likely due to the nature of the correlation classifier, since as the number of classes increases, the discrimination between consecutive targets has lower classification tolerance, becoming less reliable. Taking this into account, we consider that a direct increment in the number of stimuli without additional modifications to the BCI structure is not practical nor dependable.

4.2 On the EEG Simulator

Regarding the reliability of realistic c-VEP simulation, we first observe some non-significant inconsistencies in the grand ERP averages and power spectra of *Figures 7* and *8*. However, perhaps the most notable discrepancy concerns the results obtained from both ICAs and PCA in *Figure 5*. This figure shows significant differences in accuracy between the same feature extractors in identical setups. Since we can rule out the SNR as the origin of these inconsistencies based on the result in *Figure 9* (showing relatively little variation throughout the whole range), and the discrepancy is exclusive to component analysis algorithms, we estimate that it derives from insufficiently realistic component rankings and orthogonality among data sources. Therefore, we conclude that the biggest shortcoming identified in the simulator originate from the limitations of the simulated electrodes and head model, resulting in significantly more favourable performance in the PCA algorithm’s orthogonal transformations.

While we do acknowledge numerous areas of improvement for the EEG simulator, within the scope of this study, we consider that the operation and results achieved through a simulated approach are satisfactory. It effectively provided a genuinely practical, flexible, and robust platform for in-depth BCI analysis, with a certain degree of dependability. We believe, it is a powerful framework and a highly promising tool for streamlining the development of modern high-performance brain-computer interfaces. Undoubtedly, more sophisticated and realistic simulations will further benefit the development of BCIs in the future.

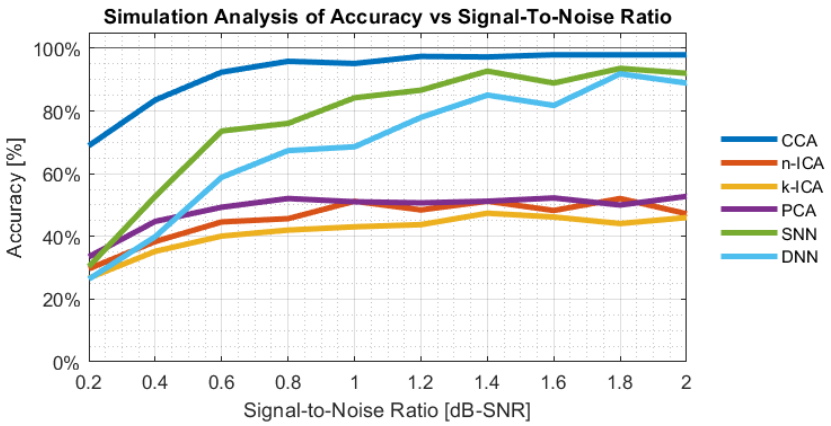

Figure 9. Analysis of the averaged influence of the simulated SNR coefficient on the accuracy of the BCI for each of the feature extractor methods in all target setups with an APA sequence. The x-axis represents the dB ratio between the signal and noise components in the EEG simulation.

4.3 Future work

The majority of the observations and results obtained in this study suggest promising methodologies and parameters, but also demand future experimentation. Particular effects of interest include the effects of the Golay and DeBruijn sequences, new paradigms to increase the number of targets per system, and the optimization of the ANN architecture in the feature extraction stage with a comparable speed to that achieved through CCA-based processing.

More sophisticated signal processing algorithms are perhaps the development with the most potential to influence the performance of c-VEP BCI systems. Although computational requirements should be taken into consideration, we consider the integration of multiple advanced methodologies for signal decoding (i.e. convolutional neural networks, fuzzy logic), classification (i.e. Support Vector Machines, k-Nearest Neighbour), and methodologies that optimize user adaptability [7], such as higher modulation frequencies and stimulation sequences that move beyond binary presentation modalities, comprise the contemporary priorities of c-VEP BCI implementations.

Finally, we consider that the insights and advancements made on realistic c-VEP simulation represent a tool that will likely provide highly significant benefits to all types of code-modulated BCIs. A simulated framework provides unparalleled practicality and control and is an approach for which we strongly encourage further development.

5. Conclusion

In this paper, we evaluated the effects of various feature extractors, modulation sequences, and the number of targets in the stimulus interface on the accuracy and information transfer rates of c-VEP BCI systems. We utilized both real and generated EEG datasets through simulation, evaluating the characteristics of the latter, and ultimately assessing its reliability. We were able to achieve a maximum information transfer rate of 127.2 bits/min with a 64-targets setup using an Almost Perfect Autocorrelation sequence for modulation, and 98.8% accuracy in a Golay-modulated 16-target system, both with a shallow neural network as a feature extractor.

Our results suggest several branching paths for the research and development of contemporary c-VEP BCI systems. Most notably our results suggest that the Golay and DeBruijn sequences, studies of which are not extensive, are highly effective for c-VEP BCI performance. We observed that the CCA and SNN methods represent the most effective feature extractors compared to multiple typical algorithms. Finally, we explored a realistic simulation framework, which not only achieved satisfactory fidelity but also provided highly valuable flexibility and exceptional accessibility to the processing pipeline analysis of a c-VEP-based BCI.

Acknowledgments

A large portion of this work was made possible thanks to [Institution]. The authors would like to thank [Institution] for their help.

References

[1] L. F. Nicolas-Alonso and J. Gomez-Gil, "Brain-Computer Interfaces, a Review," *Sensors*, 12, 1211–1279, 2012.

[2] D. J. McFarland and J. R. Wolfpaw, "Brain-Computer Interfaces for Communication and Control.," *Communications of the ACM*, 54(5), 60-66, 2011.

[3] Guangyu Bin *et al* 2011 "A high-speed BCI based on code modulation VEP," *J. Neural Eng.* 8(2), 2011.

[4] S. Nagel and M. Spuler, "Modelling the brain response to arbitrary visual stimulation patterns for a flexible high-speed Brain-Computer Interface," *PLoS One*, 13(10), 2018.

[5] Lotte F, Congedo M, Lécuyer A, Lamarche F, Arnaldi B. (2007). A review of classification algorithms for EEG-based brain-computer interfaces. Journal of neural engineering, 4(2), R1-R13.

[6] Lotte, F., Bougrain, L., Cichocki, A., Clerc, M., Congedo, M., Rakotomamonjy, A., & Yger, F. (2018). A review of classification algorithms for EEG-based brain-computer interfaces: a 10 year update. Journal of neural engineering, 15(3), 031005.

[7] S. Baillet, J. C. Mosher, and R. M. Leahy, "Electromagnetic brain mapping," *IEEE Signal Processing Mag.*, 18(6), 14-30, 2001.

[8] G. Y. Bin, X. R. Gao, Y. J. Wang, B. Hong and S. K. Gao, "VEP-based brain-computer interfaces: time, frequency, and code modulations," *IEEE Comput. Intell. Mag*., 4(4), 22-26, 2009.

[9] Zhao, Jing et al. "Comparative Study of SSVEP- and P300-Based Models for the Telepresence Control of Humanoid Robots." *PloS* one vol. 10,11 e0142168. 12 Nov. 2015.

[10] M. Spuler, W. Rosenstiel, and M. Bogdan, "Online Adaptation of a c-VEP Brain-Computer Interface(BCI) Based on Error-Related Potentials and Unsupervised Learning," *PLoS One*, 7(12), 2012.

[11] Shirzhiyan Z, Keihani A, Farahi M, Shamsi E, GolMohammadi M, Mahnam A, et al. (2019) Introducing chaotic codes for the modulation of code modulated visual evoked potentials (c-VEP) in normal adults for visual fatigue reduction. *PLoS ONE* 14(3): e0213197.

[12] B. Wittevrongel, E. Wolputte, and M. Hulle, "Code-modulated visual evoked potentials using fast stimulus presentation and spatiotemporal beamformer decoding," *Scientific Reports*, 7(1), 2017.

[13] S. Kumar and K. Vijay, "Classification of EEG Signals Using Principal Component Analysis And Support Vector Machine," in *18th Annual Symposium on Emerging Needs in Computing, Communication, Signals and Power*, 2009.

[14] Q. Wei, Y. Liu, X. Gao, Y. Wang, C. Yang, Z. Lu, and H. Gong, "A Novel c-VEP BCI Paradigm for Increasing the Number of Stimulus Targets Based on GroupingModulation With Different Codes," *Trans. Neural Systems and Rehab. Eng*., 26(6), 1178-1187, 2018.

[15] Thielen J, van den Broek P, Farquhar J, Desain P (2015) Broad-Band Visually Evoked Potentials: Re(con)volution in Brain-Computer Interfacing. PLoS ONE 10(7): e0133797.

[16] E. E. Sutter, "The brain response interface: communication through visually-induced electrical brain responses," *J. Microcomputer Applications*, 15(1), 31-45, 1992.

[17] G. Y. Bin, X. R. Gao, B. Hong and S.Gao, "An online multi-channel SSVEP-based brain-computer interface using a canonical correlation analysis method," *J. Neural Eng.* 6(4), 2009.

[18] J. T. Lindgren, A. Merlini, A. Lécuyer and F. P. Adriulli, "simBCI—A Framework for Studying BCI Methods by Simulated EEG," *Trans. Neural Systems and Rehab. Eng*., 26(11), 2096-2105, 2018.

[19] Q. Wei, S. Feng and Z. Lu, "Stimulus Specificity of Brain-Computer Interfaces Based on Code Modulation Visual Evoked Potentials," *PLoS One*, 11(5), 2016.
[20] H. A. Baseler, E. E. Sutter, S. A. Klein, and T. Carney, "The topography of visual evoked response properties across the visual field.," *Clinical Neurophysiology*, (90)1, 65-81, 1994.
[21] Tangermann, M., Müller, K. R., Aertsen, A., Birbaumer, N., Braun, C., Brunner, C., Leeb, R., Mehring, C., Miller, K. J., Müller-Putz, G. R., Nolte, G., Pfurtscheller, G., Preissl, H., Schalk, G., Schlögl, A., Vidaurre, C., Waldert, S., & Blankertz, B. (2012). Review of the BCI Competition IV. *Frontiers in neuroscience*, 6(55).
[22] T. F. Oostendorp, J. Delbeke, and D. F. Stegeman, "The conductivity of the human skull: Results of in vivo and in vitro measurements," *IEEE Trans. Biomed. Eng*., 47(11): 1487–92, 2000.
[23] M. G. Parker, K. G. Paterson, and C. Tellambura, "Golay Complementary Sequences," *ISG*, 2004
[24] G. K. Aguirre, M. G. Mattar, and L. Magis-Weinberg, "DeBruijn cycles for neural decoding," *NeuroImage*, (56)3, 1293-1300, 2011.
[25] X. Zeng, J. Q. Liu, and L. Hu, "A New Family of Codes and Generalized Kasami Sequences," in *IEEE Int. Symp. on Information Theory*, 2006.
[26] S. W. Golomb, "Shift Register Sequences –A Retrospective," *Int. Conference on Sequences and Their Applications*, 1-4, 2006.
[27] F. Rodríguez Hernández, N. C. Cortés, J. M. Rocha-Pérez and A. Sánchez, "Generation of Gold-Sequences With Applications to Spread Spectrum Systems," in *CINVESTAV-IPN*, 2000.
[28] Isaksen, J. L., Mohebbi, A., & Puthusserypady, S. (2017). Optimal pseudorandom sequence selection for online c-VEP based BCI control applications. *PloS one*, *12*(9), e0184785.
[29] X. Guo and X. Wu, "Mental EEG analysis based on independent component analysis," in *3rd Intl. Symposium on Image and Signal Processing and Analysis*, 2003.
[30] J.-i. Sato and Y. Washizawa, "Neural Decoding of Code Modulated Visual Evoked Potentials bySpatio-Temporal Inverse Filtering for Brain-Computer Interfaces," in *38th Annual Int. Conference of the IEEE Engineering in Medicine and Biology Society*, 2016.
[31] T. Jolliffle and J. Cadima, "Principal component analysis: a review and recent developments," *The Royal Society*, 374(2065), 2016.
[32] J. Knollmuller and T. A. Ensslin, "Noisy independent component analysis of auto-correlated components," 2017.
[33] S. Lekshmi, V. Selvam and M. P. Rajasekaran, "EEG signal classification using Principal Component Analysis and Wavelet Transform with Neural Network," in *Int. Conference on Communication and Signal Processing*, 2014.
[34] Kottaimalai R, Rajasekaran M, Selvam V and Kannapiran B "EEG signal classification using Principal Component Analysis with Neural Network in Brain-Computer Interface applications," *in IEEE Int. Conference on Emerging Trends in Computing, Communication, and Nanotechnology*, 2013.
[35] D. B. Malkoff, "A Neural Network for Real-Time Signal Processing," NIPS, 248-255, 1989.
[36] Billinger, M. *et al.* Is it significant? Guidelines for reporting BCI performance. in Toward Practical BCIs: Bridging the Gap from Research to Real-World Applications (eds. Allison, B. Z., Dunne, S., Leeb, R., Milan, J. D. R. & Nijholt, A.) 333–354 (Springer, 2012).